Enhanced UV photosensing properties of ZnO nanowires prepared by electrodeposition and atomic layer deposition

Rodolphe Alchaar, Houssin Makhlouf, Nadine Abboud, Sophie Tingry, Radhouane Chtourou, Matthieu Weber, Mikhael Bechelany

Enhanced UV photosensing properties of ZnO nanowires prepared by electrodeposition and atomic layer deposition

Rodolphe Alchaar[a,b,c], Houssin Makhlouf[b,d,e], Nadine Abboud[a,c], Sophie Tingry[b], Radhouane Chtourou[d] , Matthieu Weber[b] and Mikhael Bechelany[b]

[a] *Research Platform for Nanosciences and Nanotechnologies, Campus Pierre Gemayel, Lebanese University, Fanar 90239, Lebanon.*

[b] *Institut Européen des Membranes, UMR 5635 Université Montpellier, CNRS, ENSCM, Place Eugene Bataillon, F-34095 Montpellier cedex 5, France.*

[c] *Laboratory of Applied Physics, Campus Pierre Gemayel, Lebanese University, Fanar 90239, Lebanon.*

[d] *Laboratoire de Nanomatériaux et Systémes des Energies Renouvelables (LANSER), Centre de Recherche et des Technologies de l'énergie, Borj Cedria, BP 95, 2050 Hammam-Lif, Tunisia.*

[e] *Faculté des sciences de Tunis, Université Tunis El Manar, Tunis, Tunisia.*

† Corresponding authors: Mikhael Bechelany, mikhael.bechelany@univ-montp2.fr.

Abstract. A new process enabling the synthesis of ZnO and Al-doped ZnO nanowires (NWs) for photosensing applications is reported. By combining atomic layer deposition (ALD) for the seed layer preparation and electrodeposition for the NWs growth, high quality ZnO nanomaterials were prepared and tested as UV sensors. The obtained NWs are grown as arrays perpendicular to the substrate surface and present diameters between 70 and 130 nm depending on the Al doping, as seen from scanning electron microscopy (SEM) studies. Their hexagonal microstructure has been determined using X-ray diffraction and Raman spectroscopy. An excellent performance in UV sensing has been observed for the ZnO NWs

with low Al doping, and a maximal photoresponse current of 11.1 mA has been measured. In addition, initial studies on the stability have shown that the NWs photoresponse currents are stable, even after 10 UV on/off cycles.

Keywords. ZnO nanowires, Al-doping, electrochemical deposition, atomic layer deposition, photosensors.

Introduction

Zinc oxide (ZnO) is a semiconductor material presenting a wide-direct-band gap (~3.37 eV), and photodetection is one of the main applications of ZnO nanostructures. These nanomaterials have thus been the subject of intense research for their application in optoelectronic devices.[1, 2] Various ZnO "nanogeometries" have been reported in the literature, such as nanobelts, nanowires, nanoneedles, nanotetrapods, and nanocombs.[3-6] Among the one-dimensional (1D) nanostructures, ZnO nanowires are particularly interesting, as they present a high surface-to-volume ratio and quantum confinement effects, which are interesting properties for various electronics and optoelectronics applications.[7-9]

The photoconductivity can be directly linked to the surface adsorption and desorption of oxygen species. By illuminating ZnO with a ultraviolet (UV) light, electrons in the valence band acquire enough energy to cross the band gap and electron-hole pairs are generated. The photogenerated holes will act on the desorption of the oxygen species and the liberated electrons will increase the (photo)conductivity.

The photoconductivity of ZnO has been described in previous studies. For example, Wang *et al.* reported the photoconduction mechanism in a ZnO single nanowire,[10] and Zheng *et al.* studied the properties of ZnO films UV detectors.[11] Liu *et al.* investigated the effects of oxygen plasma treatments on the UV detection properties of ultrathin ZnO epitaxial films.[12] Different doping elements such as F, Al, Ga, In and Sn have been used to improve the properties of ZnO films.[13-15] A few studies have reported the application of doped ZnO nanostructures for UV photosensing. Mamat *et al.* studied the photoconductive properties of Al-doped ZnO thin films deposited by sol-gel spin-coating method [16] and Al-doped ZnO nanorod-arrays deposited using sonicated sol-gel immersion method [17].

A nucleation layer is often vital for the controlled growth of NWs array.[18, 19] ZnO NWs are generally grown using either heteroepitaxy with the appropriate single crystalline substrates (usually Al_2O_3 or GaN), or homoepitaxy on textured ZnO thin films acting as a nanowire nucleation layer.[18] However, different alternative routes have been developed for the preparation of aligned ZnO NWs arrays, including metal-organic chemical vapor deposition (MOCVD), vapor-liquid solid (VLS), pulsed laser deposition method (PLD) and solution based chemical techniques.[20-23] Electrodeposition is an alternative and attractive approach for the growth of ZnO nanostructures because of its simplicity, low cost and low processing temperature. Furthermore, this synthesis method allows for the large-scale growth of aligned ZnO nanowires on various substrates, which demonstrates the viability of the process for industrial applications.[24]

Atomic layer deposition (ALD) is a scalable vapor phase deposition technique enabling the synthesis of ultrathin films of inorganic materials, with a subnanometer thickness control.[25] The properties of the synthetized nanostructures can be tuned by adjusting

the process conditions – *e.g.* the chemistry of the precursor(s) and the co-reactants, the temperature, the number of cycles, or the nature of the substrate.[25-29]

Herein, we combine ALD and electrodeposition in order to synthesize tunable ZnO NWs. We effectively grow NWs by electrodeposition on a 20 nm thin ZnO seed layer deposited by ALD. The seed layer of ZnO is required to provide nucleation sites and control of the vertical NWs growth.[18, 19] In order to enhance the optical and electrical properties, the process was developed to achieve the doping of the ZnO nanowires with Aluminum. The effect of Al doping on the morphological, structural and optical properties of ZnO nanowires is studied in detail. Finally, the UV photoconductive response of the Al-doped ZnO NWs is determined and open prospects for their potential as UV photodetectors.

Materials and Methods

1. Materials

Zinc chloride ($ZnCl_2$), potassium chloride (KCl) and diethyl zinc (DEZ) ($Zn(CH_2CH_3)_2, 95\%$) were purchased from Sigma Aldrich and used as received. Alfa Aesar was the supplier of Aluminum chloride hexahydrate ($AlCl_3.6H_2O, 99\%$). The ITO coated glass substrates were purchased from Kintec (Hong Kong).

2. Synthesis of ZnO NWs

A home-built ALD reactor was used for the preparation of ZnO thin films. ALD was performed using sequential exposures of Diethyl Zinc (DEZ) and H_2O. The process has been reported in previous studies.[30-33] Briefly, the ALD cycle consisted of a 0.2 s pulse of DEZ, 30 s of exposure to DEZ, 60 s of purge followed by a 2 s pulse of H_2O,

30 s of exposure to H_2O and finally 60 s purge with nitrogen. The flow rate was around 100 sccm and the deposition temperature was 100 °C.

If not precised otherwise, the ZnO films synthesized were 20 nm thick and deposited on Indium Tin Oxide (ITO) substrates. Before the depositions, the substrates were cleaned by acetone and isopropanol (15 min each) in an ultrasonic bath and then rinsed with water.

Next, an electrodeposition process was carried out to grow the NWs from a supporting electrolyte consisting of 0.5 mM $ZnCl_2$ and 0.1 M KCl, with deionized water as solvent.[34] Molecular oxygen was supplied to the solution by bubbling O_2 during 45 minutes prior to the experiment, and this O_2 bubbling was maintained during the deposition process. To achieve the Al doping, $AlCl_3.6H_2O$ was added to the solution. By varying the Al/Zn atomic ratio in the electrolyte solution, ZnO NWs with different Al doping percentages were prepared (the ratios used were 0, 0.1, 0.5, 1, 2 and 5 mol%). All electrodepositions were carried out at 80°C during 150 minutes in a three-electrodes cell. The ITO substrate, the platinum plate, and the Ag/AgCl electrode were respectively used as the working electrode, the counter electrode and the reference electrode. The deposition potential was -1.0 V versus Ag/AgCl.[34] At the end of each growth period, the supported ZnO nanowires were removed from the solution and rinsed in deionized water for 20 minutes at 80 °C to eliminate any residual impurities from the surface.

3. Chemical and structural characterizations

The morphology and the microstructure of the synthesized ZnO NWs were determined using scanning electron microscopy (SEM, HITACHI S4800), energy dispersive X-Ray spectroscopy (S-4500, coupled with a Thermofisher EDX detector), Raman

spectroscopy (Horabi) and X-Ray diffraction (XRD, PANAlytical Xpert-PRO diffractometer equipped with an X'celerator detector using Ni-filtered Cu-radiation).

4. UV sensor measurement

In order to study the photodetection properties of the samples, electrical measurements were performed under dark and UV illumination. The radiation power of the 365 nm UV source illuminating the sample device was $1.87\ \mathrm{mW/cm^2}$. Silver contacts were applied to the samples surface with 5 mm separating distance in order make a measureable device and to perform the electrical measurements, as depicted in Figure 1. [35]

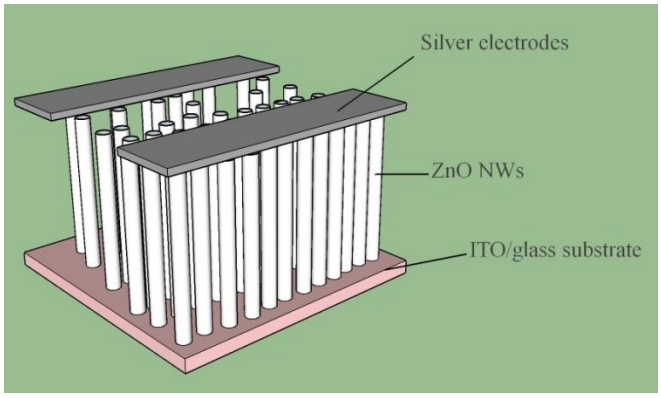

Figure 1. Schematic representation of the device with silver contacts

Sweep voltammetry and chronoamperometry measurements have been performed using a potentiostat (EG&G instruments, 265 A model). Sweep voltammetry has been carried out from -3 to 3 V with a scanning speed of $50\ \mathrm{mV/s}$. In order to extract the photoresponse current and the recovery time, chronoamperometry measurements were performed with on/off UV illumination. They have been performed at -1 V during 3000 s using the following protocol: UV off between 0 and 100 s ; UV on between 100 and 200 s ; UV off between 200 and 3000 s. The UV photoresponse data have been extracted from chronoamperometry experiments. The photoresponse current (ΔI) was

defined as the difference between current under UV illumination and current under dark, and the recovery time τ was defined as the time for the photoresponse current to drop to $1/e$ (37%) of the maximum photoresponse current. During the electrical measurements the UV cell was covered with a black box to ensure light isolation.

Results and discussion

1. Material properties

In order to study the influence of Al-doping on the properties of the synthesized ZnO NWs, the Al/Zn atomic ratio in the electrolyte solution used for the electrodeposition was varied (0, 0.1, 0.5, 1, 2 and 5 mol%). Thus, ZnO NWs with increasing Al contents could be prepared. The chemical composition for all ZnO NWs samples has been evaluated by energy dispersive X-Ray spectroscopy and the results are displayed in Table 1. The ZnO NWs synthesized are near-stoichiometric, with a slight excess of oxygen. A weak signal from Al has been detected for the doped samples, indicating that the doping was effective.

Table 1. Chemical composition of the elements present in ZnO and Al-doped ZnO samples.

Doping percentage	O (%)	Zn (%)	Al (%)
0 %	56	44	-
0.1 %	54	46	-
0.5 %	56	44	0.3
1 %	60	40	0.4
2 %	54	46	0.4
5 %	66	34	0.5

The morphology of the synthesized nanostructures has been studied by scanning electron microscopy (SEM). Figure 2 presents the top view SEM images of the ZnO NWs samples prepared using different doping percentages.

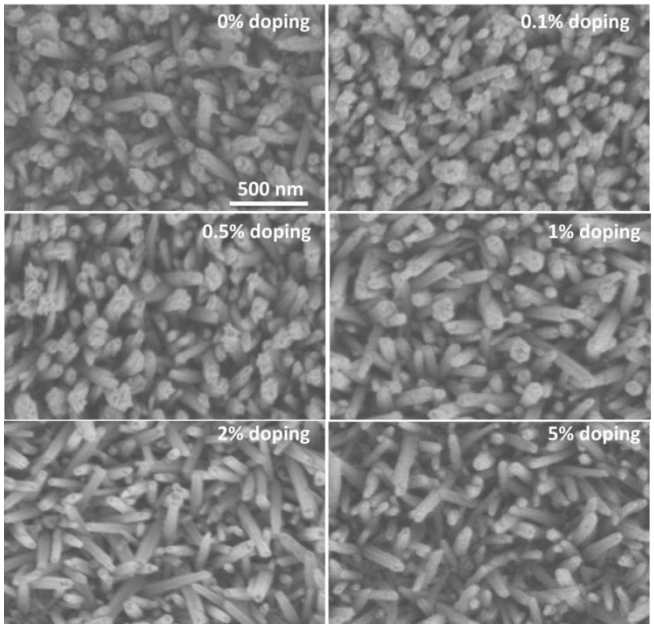

Figure 2. SEM images of ZnO NWs obtained with different Al doping percentages (indicated in the top right corner of each image).

The morphology of all samples can be described as NW arrays perpendicular to the substrates. The NW diameters increased from approximately 70 nm for the undoped NWs and 0.1 % doped NWs, to 130 nm for the 0.5 and 1 % doped samples. The diameters measured for the 2 and 5 % doped samples were 60 and 80 nm, respectively. This difference could be attributed to the increase of the growth rate and the change of the growth orientation of ZnO NWs with the incorporation of Al dopants up to 1 %.[36] The decrease of the diameter for the 2 and 5 % doped samples could be related to the deterioration of the crystallinity of the NWs (see section above).

Next, Raman spectroscopy measurements have been carried out in order to further characterize the chemical structure of the samples. Figure 3 shows the Raman spectra of ZnO and Al-doped ZnO NWs. All samples present an obvious band around 438 cm^{-1}, which can be assigned to the E_2 (high) phonon scattering mode of ZnO hexagonal structure.[37]

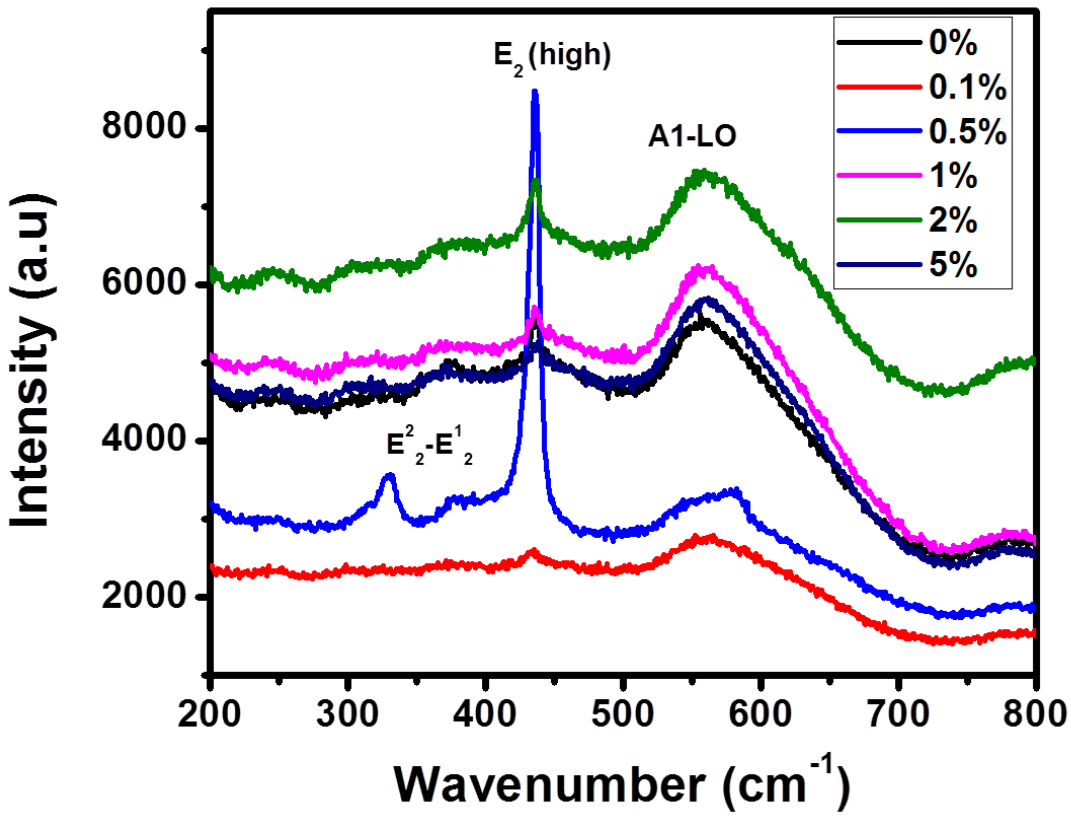

Figure 3. Raman spectra of ZnO and Al-doped ZnO NWs.

The fact that the E_2 (high) mode is sensitive to the stress within ZnO nanostructures has been reported in the literature.[38] In our samples, this E_2 peak does not show any noticeable shift between undoped and Al-doped NWs. Thus, we believe the Al dopants did not introduce excessive stress in the samples. The band at ~570 cm^{-1} corresponds to the A1 (*LO*) mode.[39] An increase of the intensity of this peak with the increasing doping percentage can be seen. As reported previously,[40] the enhancement of this

LO mode by the Al doping can be attributed to the electric field induced (EFI) Raman scattering. The band at 331 cm^{-1} observed for the 0.5 %-doped NWs can be attributed to the $E_2^2 - E_2^1$ optical phonon modes of ZnO single crystal.[41]

The microstructure of the samples has then been investigated. XRD diffraction patterns of ZnO NWs with different doping percentages are shown in Figure 4.

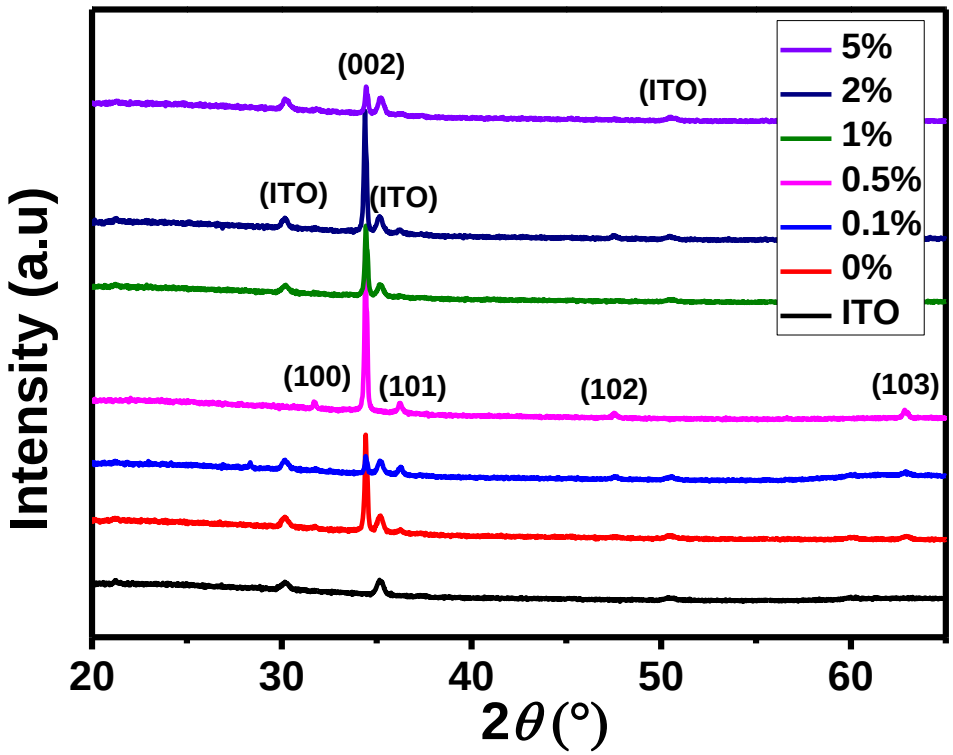

Figure 4. XRD patterns of ZnO and Al-doped ZnO NWs and ITO substrate.

The peaks observed at $31.7°, 34.4°, 36.2°, 47.5°$ and $62.9°$ correspond respectively to the (100), (002), (101), (102) and (103) planes of hexagonal ZnO. The other peaks (at $2\theta = 30.1°, 35.2°, 50.3°$) can be attributed to the ITO substrate.

The intensity of the (002) peak is stronger than the other peaks, suggesting that ZnO crystallites are highly oriented with the c-axis being perpendicular to the substrate. As compared to undoped ZnO NWs, the (002) peak intensity increased with the increase

of Al doping for 0.5% and 2% doped nanowires. However, it is observed that the peaks decreased for 0.1%, 1% and 5% doped nanowires. To understand the relationship between the concentration of the Al doping and the (002) peak intensity, a comparison of the (002) peaks of undoped ZnO NWs and ZnO NWs with 0.1%, 1% and 5% Al-doping is given in Figure 5.

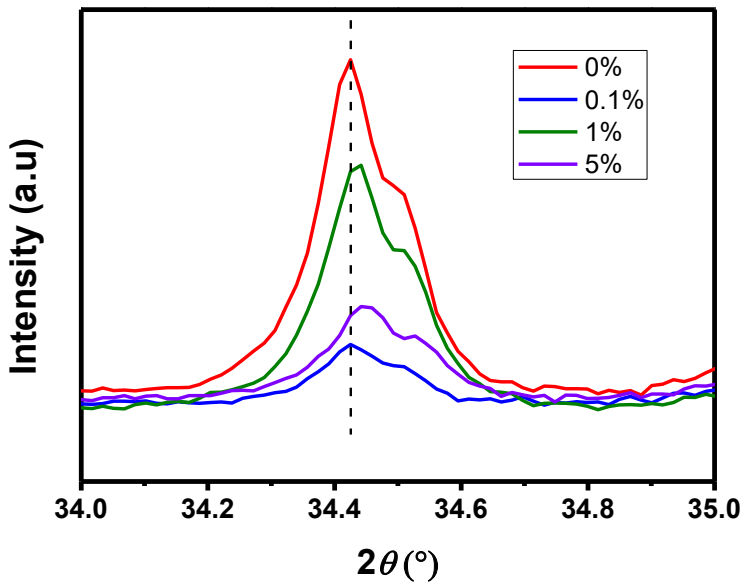

Figure 5. XRD patterns of the (002) peak of undoped ZnO NWs 0% and ZnO NWs with 0.1%, 1% and 5% Al-doping.

A shift to the large angle of diffraction peaks for 1% and 5% Al-doped ZnO NWs is observed compared with that of the undoped ZnO NWs. The shift of the two samples (1% Al and 5% Al) was found to be 0.013° and 0.025° respectively. This small shift could be attributed to the smaller atom radius of substituted Al^{3+} (0.53 Å) than that of Zn^{2+} (0.60 Å) in the ZnO lattice .[38] This shift may explain the decrease of the (002) peak intensity.

This result may be due to the deterioration in crystalline quality or segregation of aluminum in the grain boundaries at higher doping concentrations.[42] Concerning the 0.1% Al doped sample, the shift of diffraction (002) peak disappear while its intensity is weak. According to the EDX results, the atomic ratio (O\Zn) of ZnO NWs doped 0.1% Al was found to be 1.17 and the doping was not detected due to the small amount of Al (0.1%) introduced on the ZnO NWs. It is thus expected that the stoichiometry was slightly improved with less oxygen vacancies. A lack of oxygen vacancies may induce a degradation of crystalline quality.[43] As a result, the diffraction peak intensity for (002) orientation decreases.

The grain sizes reported in Table 2 were calculated using the Debye-Scherrer formula[44]:

$$D = \frac{0.9\lambda}{\beta \cos\theta} \quad (1)$$

Where *D, θ,* and λ are the mean crystallites size, the Bragg angle, and the wavelength of the incident X-ray (0.154 nm), respectively.

Table 2. Grain size of ZnO and Al-doped ZnO NWs

Doping percentage (%)	0	0.1	0.5	1	2	5
Grain size (nm)	42.3	53.2	54.4	49.3	51.3	46.4

As shown in Table 2, the size of the grains tends to get larger with increasing the Al doping up to 0.5 %, and their size decrease for higher doping concentrations. The decrease of grains size with increasing of dopant concentration may be attributed to the alternation of Zn and Al atoms which can prevent the growth of larger ZnO grains.

This suggests the improvement of the crystallinity of low Al-doping samples, and the deterioration of the crystalinity for the higher Al-dopings.

Figure 6 displays the UV-Visible absorption spectra of the ZnO NWs. No absorption features were seen in the visible region for the ZnO NWs which indicates their high purity. We observe an absorption edge at 380 nm which corresponds to the excitonic band gap of ZnO NWs. In particular, the absorption edge is blueshifted with the increase of Al doping, suggesting the broadening of the optical bandgap. Typically, the blueshift of the absorption edge of the Al-doped ZnO NWs can be associated to the increase of the carrier concentration (blocking the lowest states in the conduction band), which is known as the Burstein-Moss effect.[45, 46] In order to estimate the bandgap of the samples, $(\alpha h\nu)^2$was plotted against $h\nu$, which is known as Tauc plot, where α is the absorbance, h is planck's constant and ν is the incident light's frequency.[47] Then, the vertical segment of the plot was extrapolated to intersect with the x-axis. The value at the intersection between the extrapolated segment and the x-axis is the badngap, as depicted in Figure 7. The calculated bandgap values are shown in Table 3. No clear trend for the bandgap variation was observed between 0% and 0.5%, however, the bandgap increased for the 1, 2 and 5% doped samples from 3.22 to 3.25 eV, indicating perfect accordance with absorption results.

Table 3. Doping % of ZnO NWs and the corresponding bandgap.

Doping (%)	**0**	**0.1**	**0.5**	**1**	**2**	**5**
Bandgap (eV)	3.24	3.17	3.16	3.23	3.24	3.28

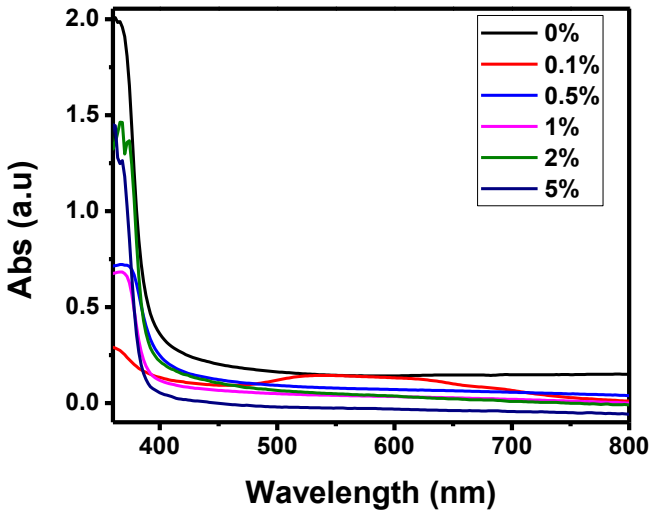

Figure 6. UV-visible absorption spectra in the wavelength range 360-800 nm for undoped and Al-doped ZnO NWs.

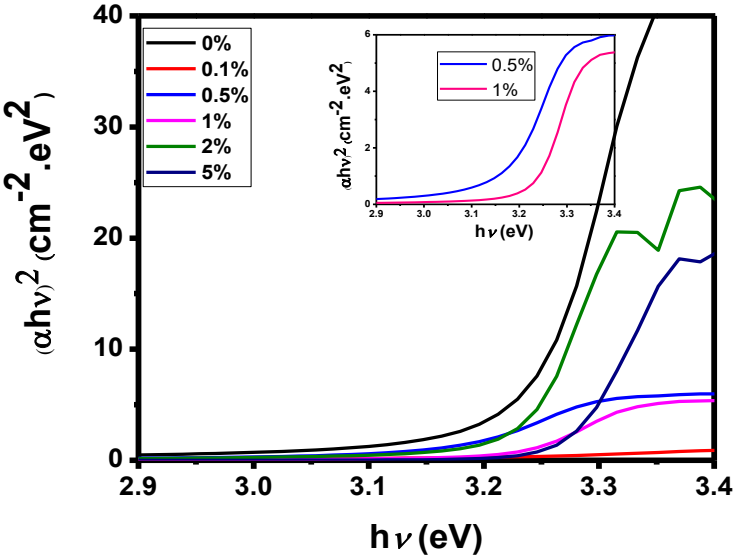

Figure 7. Tauc plots for undoped and Al-doped ZnO NWs.

2. UV sensing measurements

A high-performance photodetector should satisfy the "5S" requirements of high sensitivity, high signal-to-noise ratio, high spectral selectivity, high speed and high stability.[48] Sweep voltammetry *IV* curves of all NWs samples are shown in Figure 8. The *IV* curves shapes strongly suggest the ohmic contacts between the ZnO

nanomaterials and the Ag fingers. For the 0.1, 0.5 and 1 % Al doped Zno NWs samples, the current measured increases under UV illumination, as the Al-doping increases the carrier concentration in ZnO structures.[16] However, no difference between dark and UV currents can be seen for the 2 and 5% Al doped Zno NWs samples due to excessive Al atoms, that possibly included defects which deteriorated ZnO microstructure, as suggested by the XRD results. In fact, it is likely that the electron mobility is affected by the smaller grain sizer of these samples, and that the photocurrent properties are decreased.[16]

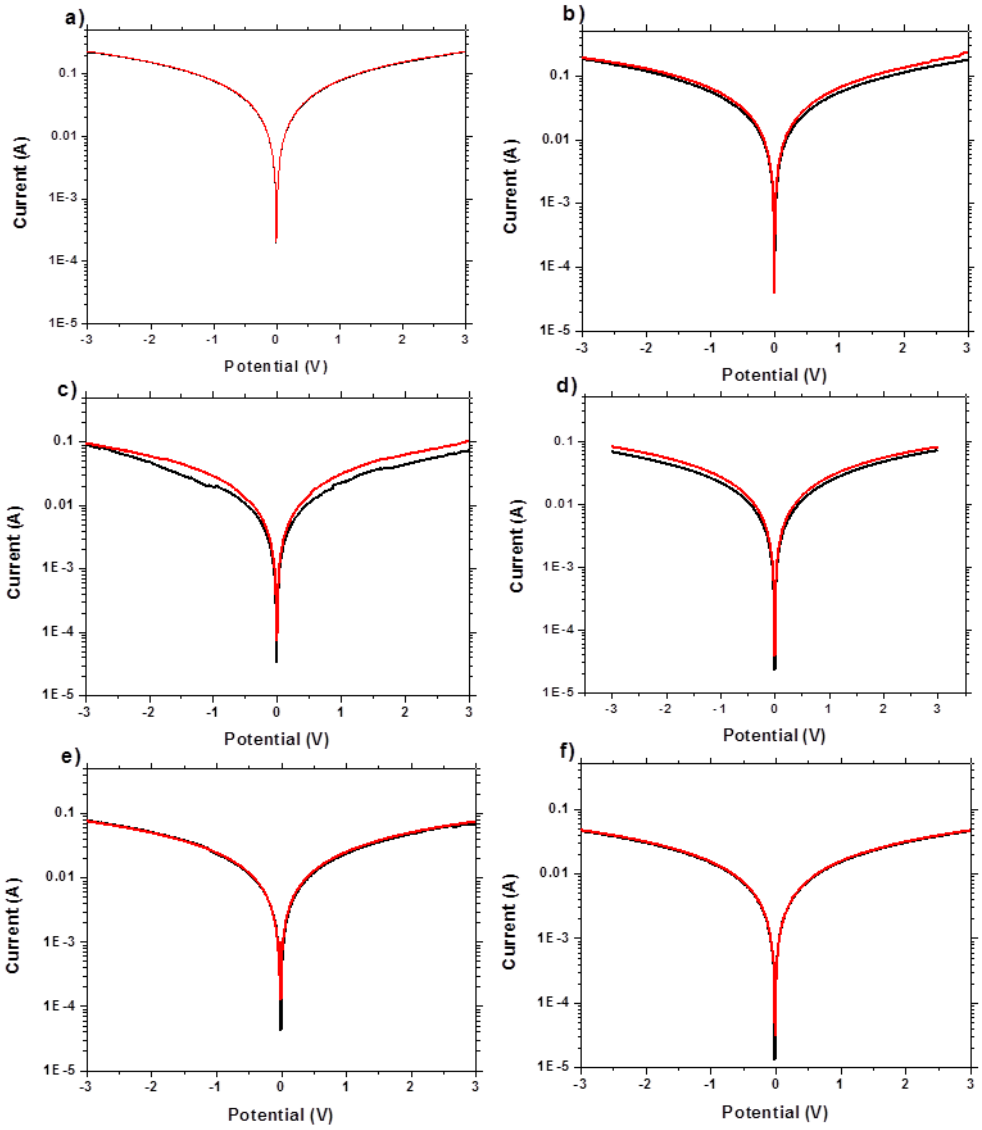

Figure 8. *IV* curves of (a) 0%, (b) 0.1%, (c) 0.5%, (d) 1%, (e) 2% and (f) 5% under dark (black curves) and UV illumination (red curves), as determined by sweep voltammetry.

Chronoamperometry measurements have been performed to study the intensity of the photocurrent as a function of time. Figure 9 depicts the intensity over time for ZnO and Al-doped ZnO NWs under UV illumination (365 nm).

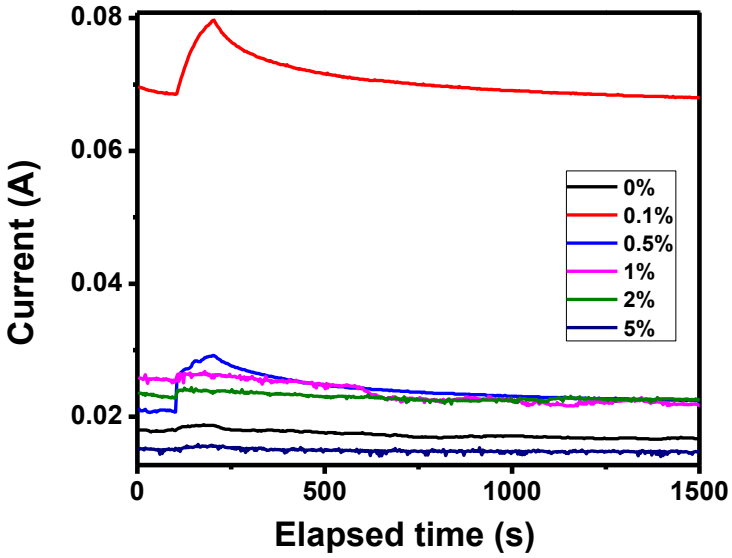

Figure 9. Intensity versus time curves for ZnO and Al-doped ZnO NWs samples under UV illumination (365 nm) between 100 and 200 s, as determined by chronoamperometry measurements.

In order to gain more understanding on the influence of Al doping on the UV photoresponse properties, the UV photoresponse and the recovery time have been extracted and plotted versus the doping percentage (Figure 10). The photoresponse current was determined by calculating the difference between I_{UV} and I_{Dark}, and the recovery time was defined as the time for the photoresponse current to drop to 37% of

its maximum value. These parameters are reported in Table 4. The UV photoresponse of a photodetector (*A/W*) is defined as a ratio between electrical output (photoresponse current) and optical input (UV source's power). The external quantum efficiency can be defined as the number of carriers circulating through a photodetector per absorbed photon and per time unit. It was calculated using the following expression:[49]

$$EQE = \frac{hc}{q\lambda}\frac{\Delta I}{PS}$$

Where ΔI is the photoresponse current, P is the light power density irradiated on the NW, S is the irradiated area of an individual NW, λ is the excitation wavelength, h is Planck's constant, c is the velocity of light and q is the electronic charge. EQE increased significantly with increasing doping percentage to 0.1%. This is due to the increase of free carriers in the lattice with the incorporation of Al. When reaching higher doping concentrations, the decreasing quantum efficiency values could be attributed to the deterioration of crystalline quality (as shown in Figure 4) which impedes the flow of carriers. Ultrahigh EQE values were also reported elsewhere and they were attributed to high quality NWs and spatial charge separation due to surface trapping of holes.[50]

Table 4. I_{Dark} and I_{UV} with the $I_{\mathrm{UV}}/I_{\mathrm{Dark}}$ current ratio at -1 V bias; UV photoresponse current and recovery time for ZnO and Al-doped ZnO samples.

Doping percentage	0 %	0.1 %	0.5 %	1 %	2 %	5 %
$\boldsymbol{I_{\mathrm{dark}}(\mathrm{A})}$	0.0179	0.0686	0.0207	0.0252	0.0228	0.01495
$\boldsymbol{I_{\mathrm{UV}}(\mathrm{A})}$	0.0187	0.0797	0.0292	0.0263	0.0244	0.01583
$\boldsymbol{I_{\mathrm{UV}}/I_{\mathrm{Dark}}}$	1.04	1.16	1.41	1.04	1.07	1.06
$\boldsymbol{\Delta I\ (\mathrm{mA})}$	0.8	11.1	8.5	1.1	1.6	0.88

UV photoresponse (A/W)	0.95	8.48	6.99	1.47	2.85	0.94
$\boldsymbol{T}$ **(s)**	31	211	502	282	394	472
EQE ($* \mathbf{10^{10}}\ \boldsymbol{W.nm.A-1}$)	3.78	52.4	2.91	0.377	10.3	3.2

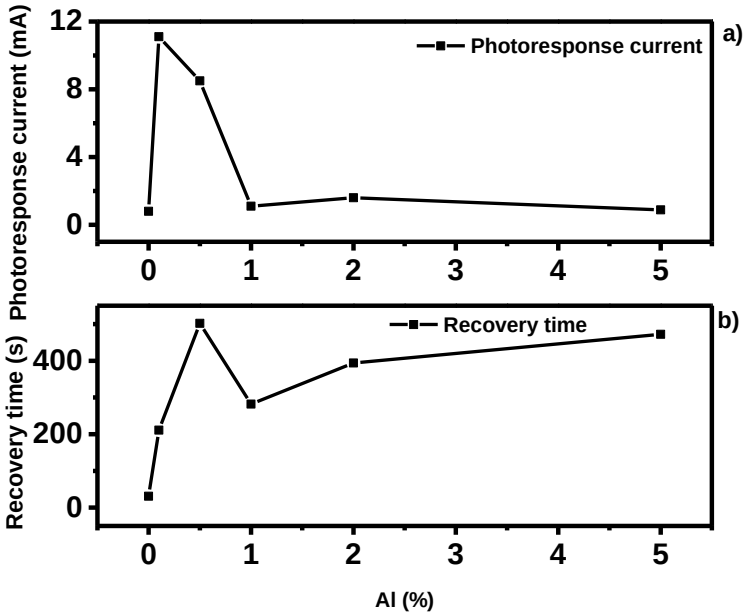

Figure 10. UV photocurrent (a) and recovery time (b) versus Al-doping percentage.

High UV photoresponse and low recovery time values are the most important parameters for UV sensors, because they indicate a high sensitivity and a high speed. From the results presented in Figure 10, it can be concluded that the optimal UV sensing performances are observed for the 0.1 % doped ZnO NWs sample. In fact, this sample clearly presents the highest photoresponse current (ΔI), UV photoresponse and quantum efficiency (11.1 mA; 8.48 A/W; $5.24 * 10^{11}$)W.nm.A^{-1}), and it also has the second lowest recovery time values (211 s). Undoped ZnO exhibits low n-type conductivity due to the low carrier concentrations in the NWs, whereas Al-doped ZnO has carrier concentrations in excess, enhancing the n-type conductivity. Thus, the photocurrent response of undoped ZnO is very low (0.8 mA) compared to the doped

ZnO NWs (11.1 mA). The decrease of the photodetection properties in the other Al doped ZnO NWs (between 1 and 5 % atom) may be attributed to the defects formed by the excess of Al atoms. The recovery time for the 0.1% doped ZnO NWs obtained in this study is shorter than that reported in the literature,[12, 51] and overall, the performances observed for our samples are comparable to the ones reported by Mamat *et al.* for ZnO nanorods samples.[17] This shows that the alternative approach developed in this work is a viable new route for the synthesis of ZnO nanosensors.

Next, the stability of the sample with 0.1% doping has been tested. 10 cycles of 'on/off' UV illumination have been carried out by chronoamperometry. The cycles are separated by 1000 s. The stability curve for the 0.1 % sample is shown in Figure 11a (over 10 cycles).

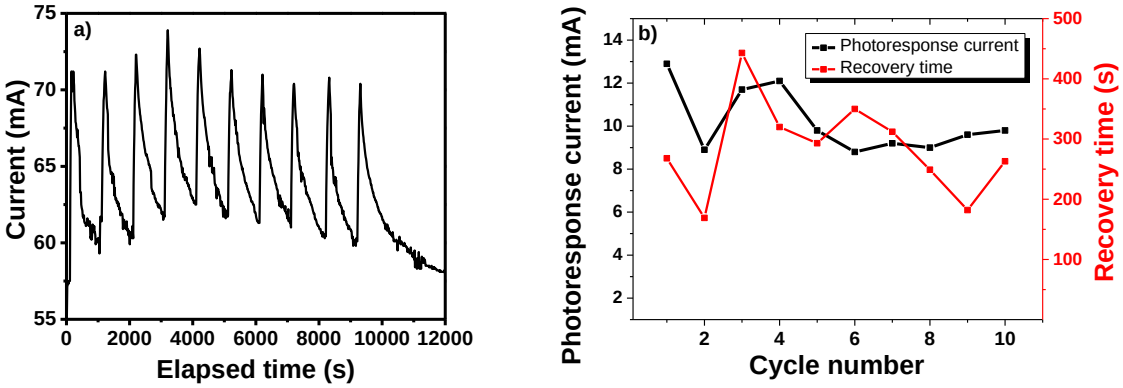

Figure 11. (a) Device stability test of 0.1% Al-doped ZnO NWs over 10 cycles and (b) photoresponse current and recovery time vs cycle number for the 0.1% Al-doped ZnO NWs sample.

Table 5. UV photoresponse current and recovery time against number of cycles for 0.1% doped sample.

Cycle number	1	2	3	4	5	6	7	8	9	10
ΔI (mA)	12.9	8.9	11.7	12.1	9.8	8.8	9.2	9	9.6	9.8
T (s)	268	169	443	320	293	350	312	249	182	263

This initial stability study shows that the photoresponse current varied between 10 and 30 % at the first cycles, but became stable after the 5th cycle, as can be seen in Figure 11b and Table 5. On the other side, the recovery time did not show any relevant stabilization during the test, which may be due to the fact that repeated UV illuminations induce changes in the electrical properties and/or the crystallinity of ZnO NWs.[52] Further studies are however necessary to confirm this assumption.

Conclusions

In this work, a novel process for the synthesis of ZnO and Al-doped ZnO NWs has been described. The new route has been used to prepare NWs arrays on TCO substrates, and the ZnO based nanomaterials were then tested as UV sensors. We used ALD for the seed layer preparation and electrodeposition for the NWs growth. The ZnO NWs presented a hexagonal microstructure and were grown perpendicularly to the substrates surface. They offered diameter between 70 and 130 nm depending on the Al doping concentration. Excellent UV photocurrents and short recovery time values have been measured for all samples. The study revealed that the 0.1 % Al-doped ZnO NWs exhibited the highest photocurrent values for UV detection (up to 11.1 mA). This novel technique combining ALD and electrodeposition is therefore a promising new route for the preparation of Al-doped ZnO NWs, since it allows for the scalable fabrication of UV sensors with high sensitivity, fast speed and stability.

Acknowledgements

We acknowledge the National Council for Scientific Research of Lebanon for funding.

References

[1] Kim DC, Jung BO, Kwon YH, Cho HK (2011) Highly Sensible Zno Nanowire Ultraviolet Photodetectors Based on Mechanical Schottky Contact. J. Electrochem. Soc 159:K10-K14
[2] Li Y, Gong J, Deng Y (2010) Hierarchical Structured Zno Nanorods on Zno Nanofibers and Their Photoresponse to Uv and Visible Lights. Sens. Actuator A-Phys 158:176-182
[3] Wan Q, Li Q, Chen Y, Wang T-H, He X, Li J, Lin C (2004) Fabrication and Ethanol Sensing Characteristics of Zno Nanowire Gas Sensors. Appl. Phys. Lett. 84:3654-3656
[4] Zhu Y, Zhang H, Sun X, Feng S, Xu J, Zhao Q, Xiang B, Wang R, Yu D (2003) Efficient Field Emission from Zno Nanoneedle Arrays. Appl. Phys. Lett. 83:144-146
[5] Xiangfeng C, Dongli J, Djurišic AB, Leung YH (2005) Gas-Sensing Properties of Thick Film Based on Zno Nano-Tetrapods. Chem. Phys. Lett. 401:426-429
[6] Leung Y, Djurišić A, Gao J, Xie M, Wei Z, Xu S, Chan W (2004) Zinc Oxide Ribbon and Comb Structures: Synthesis and Optical Properties. Chem. Phys. Lett. 394:452-457
[7] Viter R, Abou Chaaya A, Iatsunskyi I, Nowaczyk G, Kovalevskis K, Erts D, Miele P, Smyntyna V, Bechelany M (2015) Tuning of Zno 1d Nanostructures by Atomic Layer Deposition and Electrospinning for Optical Gas Sensor Applications. Nanotechnology 26: 105501
[8] Viter R, Iatsunskyi I, Fedorenko V, Tumenas S, Balevicius Z, Ramanayicius A, Balme S, Kempinski M, Nowaczyk G, Jurga S, Bechelany M (2016) Enhancement of Electronic and Optical Properties of Zno/Al2o3 Nanolaminate Coated Electrospun Nanofibers. J. Phys. Chem. C 120:5124-5132
[9] Wang ZL (2009) Ten Years' Venturing in Zno Nanostructures: From Discovery to Scientific Understanding and to Technology Applications. Chin. Sci. Bull. 54:4021-4034
[10] Wang ZL (2009) Zno Nanowire and Nanobelt Platform for Nanotechnology. Mater. Sci. Eng. R-Rep. 64:33-71
[11] Zheng X, Li QS, Zhao J, Chen D, Zhao B, Yang Y, Zhang LC (2006) Photoconductive Ultraviolet Detectors Based on Zno Films. Appl. Surf. Sci. 253:2264-2267
[12] Liu M, Kim HK (2004) Ultraviolet Detection with Ultrathin Zno Epitaxial Films Treated with Oxygen Plasma. Appl. Phys. Lett. 84:173-175
[13] Bae SY, Na CW, Kang JH, Park J (2005) Comparative Structure and Optical Properties of Ga-, in-, and Sn-Doped Zno Nanowires Synthesized Via Thermal Evaporation. J. Phys. Chem. B 109:2526-2531
[14] Baka O, Azizi A, Velumani S, Schmerber G, Dinia A (2014) Effect of Al Concentrations on the Electrodeposition and Properties of Transparent Al-Doped Zno Thin Films. J. Mater. Sci. Mater. Electron. 25:1761-1769
[15] Ilican S, Caglar Y, Caglar M, Yakuphanoglu F (2008) Structural, Optical and Electrical Properties of F-Doped Zno Nanorod Semiconductor Thin Films Deposited by Sol–Gel Process. Appl. Surf. Sci. 255:2353-2359
[16] Mamat M, Sahdan M, Khusaimi Z, Ahmed AZ, Abdullah S, Rusop M (2010) Influence of Doping Concentrations on the Aluminum Doped Zinc Oxide Thin Films Properties for Ultraviolet Photoconductive Sensor Applications. Opt. Mater. 32:696-699

[17] Mamat MH, Khalin MIC, Mohammad NNHN, Khusaimi Z, Md Sin ND, Shariffudin SS, Zahidi MM, Mahmood MR (2012) Effects of Annealing Environments on the Solution-Grown, Aligned Aluminium-Doped Zinc Oxide Nanorod-Array-Based Ultraviolet Photoconductive Sensor. J Nanomater. 8: 189279
[18] Greene LE, Law M, Tan DH, Montano M, Goldberger J, Somorjai G, Yang P (2005) General Route to Vertical Zno Nanowire Arrays Using Textured Zno Seeds. Nano Lett. 5:1231-1236
[19] J. F. Conley J, Stecker L, Ono Y (2005) Directed Assembly of Zno Nanowires on a Si Substrate without a Metal Catalyst Using a Patterned Zno Seed Layer. Nanotechnology 16:292
[20] Lee W, Jeong M-C, Myoung J-M (2004) Catalyst-Free Growth of Zno Nanowires by Metal-Organic Chemical Vapour Deposition (Mocvd) and Thermal Evaporation. Acta Mater. 52:3949-3957
[21] Li SY, Lin P, Lee CY, Tseng TY (2004) Field Emission and Photofluorescent Characteristics of Zinc Oxide Nanowires Synthesized by a Metal Catalyzed Vapor-Liquid-Solid Process. J J. Appl. Phys. 95:3711-3716
[22] Sun Y, Fuge GM, Ashfold MN (2004) Growth of Aligned Zno Nanorod Arrays by Catalyst-Free Pulsed Laser Deposition Methods. Chem. Phys. Lett. 396:21-26
[23] Wang M, Ye C-H, Zhang Y, Wang H-X, Zeng X-Y, Zhang L-D (2008) Seed-Layer Controlled Synthesis of Well-Aligned Zno Nanowire Arrays Via a Low Temperature Aqueous Solution Method. J. Mater. Sci. Mater. Electron. 19:211-216
[24] Sachindra Nath Das JPK, Junjie Xiong and Jae-Min Myoung (2012) Synthesis of Zno Nanowire by Mocvd Technique: Effect of Substrate and Growth Parameter. Nanowires - Recent advances
[25] Leskelä M, Ritala M (2002) Atomic Layer Deposition (Ald): From Precursors to Thin Film Structures. Thin Solid Films 409:138-146
[26] George SM (2009) Atomic Layer Deposition: An Overview. Chem. Rev. 110:111-131
[27] Weber M, Verheijen M, Bol A, Kessels W (2015) Sub-Nanometer Dimensions Control of Core/Shell Nanoparticles Prepared by Atomic Layer Deposition. Nanotechnology 26:094002
[28] Weber MJ, Mackus AJ, Verheijen MA, van der Marel C, Kessels WM (2012) Supported Core/Shell Bimetallic Nanoparticles Synthesis by Atomic Layer Deposition. Chem. Mater. 24:2973-2977
[29] Marichy C, Bechelany M, Pinna N (2012) Atomic Layer Deposition of Nanostructured Materials for Energy and Environmental Applications. Adv. Mater. 24:1017-1032
[30] Whitby JA, Ostlund F, Horvath P, Gabureac M, Riesterer JL, Utke I, Hohl M, Sedlacek L, Jiruse J, Friedli V, Bechelany M, Michler J (2012) High Spatial Resolution Time-of-Flight Secondary Ion Mass Spectrometry for the Masses: A Novel Orthogonal Tof Fib-Sims Instrument with in Situ Afm. Adv. Mater. Sci. Eng. 2012: 180437
[31] Elias J, Bechelany M, Utke I, Erni R, Hosseini D, Michler J, Philippe L (2012) Urchin-Inspired Zinc Oxide as Building Blocks for Nanostructured Solar Cells. Nano Energy 1:696-705
[32] Elias J, Utke I, Yoon S, Bechelany M, Weidenkaff A, Michler J, Philippe L (2013) Electrochemical Growth of Zno Nanowires on Atomic Layer Deposition Coated Polystyrene Sphere Templates. Electrochim. Acta 110:387-392
[33] Baitimirova M, Viter R, Andzane J, van der Lee A, Voiry D, Iatsunskyi I, Coy E, Mikoliunaite L, Tumenas S, Zaleski K, Balevicius Z, Baleviciute I, Ramanaviciene A, Ramanavicius A, Jurga S, Erts D, Bechelany M (2016) Tuning of Structural and Optical Properties of Graphene/Zno Nanolaminates. J. Phys. Chem. C 120:23716-23725
[34] Makhlouf H, Messaoudi O, Souissi A, Assaker IB, Oueslati M, Bechelany M, Chtourou R (2015) Tuning of Ag Doped Core− Shell Zno Nws/Cu2o Grown by Electrochemical Deposition. Mater. Res. Express 2:095002
[35] Nayak AP, Lin T-C, Islam MS (2012) UV and Oxygen Sensing Properties of Zno Nanowires Grown on Glass Using Ultrasound. Nanosci. Nanotechnol. Lett. 4:977-982
[36] Kim KH, Utashiro K, Abe Y, Kawamura M (2014) Structural Properties of Zinc Oxide Nanorods Grown on Al-Doped Zinc Oxide Seed Layer and Their Applications in Dye-Sensitized Solar Cells. Materials 7:2522-2533
[37] Jothilakshmi R, Ramakrishnan V, Thangavel R, Kumar J, Sarua A, Kuball M (2009) Micro-Raman Scattering Spectroscopy Study of Li-Doped and Undoped Zno Needle Crystals. J. Raman Spectrosc. 40:556-561

[38] Liu Y, Zhang H, An X, Gao C, Zhang Z, Zhou J, Zhou M, Xie E (2010) Effect of Al Doping on the Visible Photoluminescence of Zno Nanofibers. J. Alloys Compd. 506:772-776
[39] Souissi A, Sartel C, Sayari A, Meftah A, Lusson A, Galtier P, Sallet V, Oueslati M (2012) Zn-and O-Polar Surface Effects on Raman Mode Activation in Homoepitaxial Zno Thin Films. Solid State Commun. 152:794-797
[40] Tzolov M, Tzenov N, Dimova-Malinovska D, Kalitzova M, Pizzuto C, Vitali G, Zollo G, Ivanov I (2000) Vibrational Properties and Structure of Undoped and Al-Doped Zno Films Deposited by Rf Magnetron Sputtering. Thin Solid Films 379:28-36
[41] Souissi A, Marzouki A, Sayari A, Sallet V, Lusson A, Oueslati M (2011) Origin of the Raman Mode at 379 Cm− 1 Observed in Zno Thin Films Grown on Sapphire. J. Raman Spectrosc. 42:1574-1577
[42] Zhao J-L, Li X-M, Bian J-M, Yu W-D, Zhang C-Y (2005) Growth of Nitrogen-Doped P-Type Zno Films by Spray Pyrolysis and Their Electrical and Optical Properties. J. Cryst. Growth 280:495-501
[43] Jin B, Bae S, Lee S, Im S (2000) Effects of Native Defects on Optical and Electrical Properties of Zno Prepared by Pulsed Laser Deposition. Mater. Sci. Eng., B 71:301-305
[44] Langford JI, Wilson A (1978) Scherrer after Sixty Years: A Survey and Some New Results in the Determination of Crystallite Size. J. Appl. Crystallogr. 11:102-113
[45] Burstein E (1954) Anomalous Optical Absorption Limit in Insb. Physical Review 93:632
[46] Moss T (1954) The Interpretation of the Properties of Indium Antimonide. Proc. Phys. Soc. London, Sec. B 67:775
[47] Tauc J, Grigorovici R, Vancu A (1966) Optical Properties and Electronic Structure of Amorphous Germanium. Phys. Status Solidi (b) 15:627-637
[48] Liao M, Sang L, Teraji T, Imura M, Alvarez J, Koide Y (2012) Comprehensive Investigation of Single Crystal Diamond Deep-Ultraviolet Detectors. Jpn. J. Appl. Phys. 51:090115
[49] Li L, Lee PS, Yan C, Zhai T, Fang X, Liao M, Koide Y, Bando Y, Golberg D (2010) Ultrahigh-Performance Solar-Blind Photodetectors Based on Individual Single-Crystalline In2ge2o7 Nanobelts. Adv. Mater. 22:5145-5149
[50] Hu L, Yan J, Liao M, Wu L, Fang X (2011) Ultrahigh External Quantum Efficiency from Thin Sno2 Nanowire Ultraviolet Photodetectors. Small 7:1012-1017
[51] Zheng XG, Li QS, Zhao JP, Chen D, Zhao B, Yang YJ, Zhang LC (2006) Photoconductive Ultraviolet Detectors Based on Zno Films. Appl. Surf. Sci. 253:2264-2267
[52] Soleimanpour A, Hou Y, Jayatissa AH (2011) The Effect of Uv Irradiation on Nanocrysatlline Zinc Oxide Thin Films Related to Gas Sensing Characteristics. Appl. Surf. Sci. 257:5398-5402